Materials & Design 250 (2025) 113636

Contents lists available at ScienceDirect

Materials & Design

journal homepage: www.elsevier.com/locate/matdes

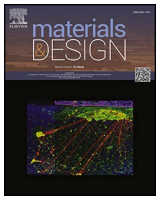

A tunable encoder with circular dichroism and polarization encoding function based on a layered metastructure in the GHz range

Chuan-Qi Wu, Jun-Yang Sui, Qi Chen, Xing-Zhou Tang *, Hai-Feng Zhang *

College of Electronic and Optical Engineering & College of Flexible Electronics (Future Technology), Nanjing University of Posts and Telecommunications, Nanjing 210023, China

ARTICLE INFO

Keywords:
Polarization conversion
Circular dichroism
Encoder
Yttrium iron garnet
Magnetized plasma
Layered metastructure

ABSTRACT

In this paper, based on a layered metastructure, a tunable encoder capable of circular dichroism (CD) and polarization conversion (PC) is researched, which contains one common medium, magnetized plasma, and yttrium iron garnet (YIG). The linear polarization waves (LPWs) are elected as incident waves. The incident angle and external magnetic field intensity are θ and H_O. A modulable dielectric layer (MDL), composed of YIG, is optionally added to the preceding item of the given metastructure, which owns a certain thickness. By adjusting the proper θ, H_O, and adding the MDL, the CD can be obtained at a certain frequency point, where the right-handed circular polarization waves (CPWs) and left-handed CPWs have different reflections. Meanwhile, the LPWs can be converted to CPWs or other polarization waves in a specific frequency band. Furthermore, the θ and addition of the MDL are considered as the first and second logic levels, respectively, to form four logic codes, which can realize the PC from LPWs to CPWs or LPWs within the same specific frequency band. Hence, the designed encoder has a promising potential in the precise control of PC in the special bandwidth, which can provide excellent support for the research of tunable and diverse polarization splitters and selectors.

1. Introduction

The polarization forms of electromagnetic waves (EWs) can be divided into linear polarization waves (LPWs), circular polarization waves (CPWs), and elliptical polarization waves (EPWs) [1], which are controlled by the phase and amplitude of the electric field intensity based on a specific time-varying law [2]. Special polarization forms of EWs always play a key role in many fields such as privacy protection [3] and EWs communication [4,5]. Among these fields, CPWs, classified as right-handed CPWs (RHCPWs), and left-handed CPWs (LHCPWs), can make a great difference in realizing multipath interference and decreasing polarization loss [6,7]. Moreover, Given that LPWs have the characteristics of good directivity, high signal strength, and strong data transmission efficiency, they are crucial for improving signal quality, receiving efficiency, and optimizing antenna design [8,9]. Therefore, it is essential to regulate the polarization forms of EWs, accurately and conveniently. By converting special controllable parameters to logic levels, encoders have great potential to reach accurate polarization conversion (PC) and information propagation.

With the rapid development of society, the digital circuit has been used in a wide range of applications such as information propagation and wireless communication [10,11]. Encoding is one of the important parts of the digital circuit, which is defined as the process of converting information from one form or format to another [12]. So, a device with the related function can be called an encoder. For the electromagnetic field, the encoder also has become a research hotspot and owned a broad application [13], Park et al. proposed multiple-bit encodings by changing the etch parameters of multilayer porous silicon in the optical reflectivity spectrum [14], whose wavelengths and amplitudes were controllable. Wang et al. investigated a smart bilayer material based on a tungsten-doped vanadium dioxide [15], which could realize multilevel information encryption by information encoding. Li et al. presented an optical polarization encoder composed of graphene-loaded plasmonic metasurfaces [16], which was capable of fulfilling all polarization forms of reflected EWs by adjusting gate voltages and polarization forms of incident EWs. Rao et al. studied a tunable polarization encoder capable of PC and circular dichroism (CD) [17], which made use of the tunability of indium antimonide to realize the conversion from LPWs to all polarization forms. Unfortunately, most research about encoding focuses on electromagnetic propagation or information imaging, ignoring its potential for PC. These few types of research about polarization encoding are limited to PC at a special single-frequency point, owning

* Corresponding authors.
E-mail addresses: xztang@njupt.edu.cn (X.-Z. Tang), hanlor@njupt.edu.cn (H.-F. Zhang).

https://doi.org/10.1016/j.matdes.2025.113636
Received 15 November 2024; Received in revised form 27 December 2024; Accepted 15 January 2025
Available online 16 January 2025
0264-1275/© 2025 The Author(s). Published by Elsevier Ltd. This is an open access article under the CC BY-NC-ND license (http://creativecommons.org/licenses/by-nc-nd/4.0/).

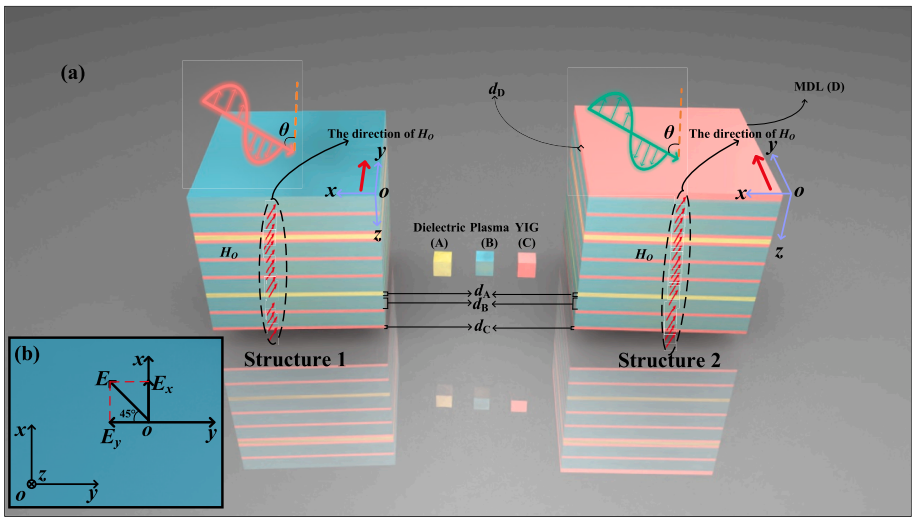

Fig. 1. **(a)** The schematic diagrams of the presented encoder, where Structure 1 is the absence of the MDL, and Structure 2 is the addition of the MDL. **(b)** the electric field (E) of the incident EWs, being at 45° to the $-y$-axis, is decomposed into the components E_y and E_x, where E_x represents the TM waves, and E_y denotes the TE one.

huge obstacles in real applications. Therefore, it is essential to propose tunable encoders, realizing special PCs in a broad frequency range, which can provide a great possibility in practical application and benefit information communication [18].

In recent years, EWs have been used more and more widely based on metamaterial or metastructure, which involve energy conversion and transmission, physical quantity detection, waveform reshaping, and other fields [19–24]. Among them, the CD of EWs is impossible to ignore, where the general definition of CD refers to the difference in the absorption of LHCPWs and RHCPWs by materials [25]. Essentially, the CD of EWs is the modulation of RHCPWs and LHCPWs to make their propagation characteristics different, meaning that the reflection difference of RHCPWs and LHCPWs, a part of the propagation characteristics, can become obvious evidence of the absorption difference between RHCPWs and LHCPWs. The incident LPWs can be considered to be composed of RHCPWs and LHCPWs. Therefore, the conversion from LPWs to RHCPWs and LHCPWs with different reflections can be viewed as the special fulfillment of the CD [26].

In this paper, a tunable encoder with CD at a single frequency point and PC in a special frequency range is proposed, which constitutes one common medium, magnetized plasma (MP), and yttrium iron garnet (YIG). The proposed encoder based on the layered metastructure can generate electromagnetic band gap and energy localization [27], which can make different changes in the phases of transverse magnetic (TM) [28] and transverse electric (TE) waves [28], respectively. Firstly, the incident angle and external magnetic field intensity are defined as θ and H_O in turn. Then, the modulable dielectric layer (MDL) is composed of YIG with a certain thickness, which can be selectively added to the preceding item of the given metastructure. Due to the ingenious arrangements for MP and YIG, the H_O, θ, and addition of the MDL can make a great effect on the phase difference ($\Delta\varphi$) between TE and TM waves, and amplitudes of the electric field intensity, attaining special PC between incident and reflected EWs. In addition, what can be called CD is that the RHCPWs and LHCPWs, converted from the same LPWs, have different propagation characteristics when propagating in the same structure [29]. Therefore, through investigating the influences of the θ, H_O, and thickness of the MDL on PC, the CD can be attained at a single frequency point, where the RHCPWs and LHCPWs can be converted by LPWs and have different reflections. At the same time, the PC from LPWs to CPWs and other polarization waves can be fulfilled within a certain frequency band. Moreover, the θ of 56°and the addition of the special MDL are defined as the first and second input logic levels "1″, respectively, while the θ of 89°and the absence of the MDL are deemed as the first and second input logic levels "0", severally. By making the above logic levels into specific combinations, the conversion from LPWs to LPWs and CPWs can be selected, expediently and precisely, in the range of 26.95 to 28.07 GHz. By associating special logic levels of θ and MDL with different PCs in a broad frequency range, the presented encoder not only owns a broad application value but also has great advantages in information transmission and storage.

2. Models and theories

As plotted in Fig. 1(a), the given configuration of the encoder owns two situations, which are divided into Structures 1 and 2 according to whether the MDL is added or not in the antecedent. The considered incident EWs are LPWs, whose front view of the electric field E is displayed in Fig. 1(b). The E is parallel to the x-y plane, and its direction is at the angle of 45° to the $+x$-axis. As a result, the E can be divided into E_x and E_y components in the $+x$- and $-y$-axis, which can generate the TE and TM waves with the same electromagnetic intensity. When the EWs incident, the incident angle is thought of as θ to the x-y plane. The given encoder contains A, B, and C, which stand for common dielectric A, MP, and YIG, respectively. For the addition of the MDL, it is deemed as D, comprising YIG with a different thickness from C. With the special arrangements and orders of A, B, C, and D, Structure 1 can be represented as $\{(BC)^2A(CB)^3A(BC)^2\}$, and the $\{D(BC)^2A(CB)^3A(BC)^2\}$ is on behalf of Structure 2. The two structures are all based on the transfer matrix method of layered structure theory [30,31], where the thicknesses of four media are defined as d_A, d_B, d_C, and d_D, respectively. Here, the d_A, d_B, d_C, and d_D are determined to be $d_A = 3$ mm, $d_B = 10$ mm, $d_C = 2.05$ mm, and $d_D = 2.59$ mm. In addition, to meet the needs of the computing transfer matrix method, the dielectric constant of A is assigned $\varepsilon_A = 7$ [17], and the magnetic permeability of A is defined as $\mu_A = 1$ [17]. Given the tunability of H_O for MP and YIG, the value of H_O is fixed as 8730 Oe, which is directed along the $+y$-axis. Moreover, due to the particularities of MP and YIG, they can be described as anisotropic media, whose special dielectric or permeability function can be obtained from Refs. [30,31], respectively. For MP and YIG, the magnetic permeability of MP and the dielectric constant of YIG are fixed as $\mu_B = 1$ [30] and $\varepsilon_C = 15$ [31]. Then, by adjusting the external H_O, the MP and YIG can vary the phases of the TM and TE waves to some extent, respectively. Then, under the arrangements of $(BC)^2$ and $(BC)^3$, and the interposition of A, it is possible for the proposed encoder to realize special PCs in a certain frequency band, which can used for the CD at a certain frequency point. Furthermore, by converting the θ and addition of the MDL into certain

logic levels, and adjusting the H_O to improve the phase difference between the TE and TM waves, the presented encoder can, accurately and handily, fulfill particular PCs over a wide frequency range.

To satisfy the computational requirements of the transfer matrix methods of MP and YIG, the external magnetic field needs to be varied. The specific formula is as follows [32]:

$$\boldsymbol{B_O}=\mu_0\boldsymbol{H_O}+\boldsymbol{M} \tag{1}$$

Due to the direction of the external H_O along the $+y$-axis, the YIG can be described as an anisotropic medium, whose effective permittivity is a tensor. The tensor is shown as follows [33]:

$$\widehat{\boldsymbol{\mu}}_f=\begin{bmatrix}\mu_r & 0 & j\mu_k\\ 0 & 1 & 0\\ -j\mu_k & 0 & \mu_r\end{bmatrix} \tag{2}$$

where

$$\mu_r=1+\frac{\omega_m(\omega_0-j\alpha\omega)}{(\omega_0-j\alpha\omega)^2-\omega^2} \tag{2-1}$$

$$\mu_k=\frac{\omega_m\omega}{(\omega_0-j\alpha\omega)^2-\omega^2} \tag{2-2}$$

$$\mu_{\mathrm{TE}}=\frac{\mu_r^2+(j\mu_k)^2}{\mu_r} \tag{2-3}$$

$$\mu_{\mathrm{TM}}=1 \tag{2-4}$$

where $\alpha=0.0002$ is the damping constant, j denotes a unit imaginary number, and ω is on behalf of the angular frequency of EWs. Moreover, $\omega_0=2\pi f_0$ is the resonance frequency [33], where $f_0=2.8\times10^6\times H_O$ and $\omega_{\mathrm{m}}=2\pi f_{\mathrm{m}}$ stands for the circular frequency [33], where $f_{\mathrm{m}}=2.8\times10^6\times M_s$. The M_s, representing saturation magnetization, is fixed as 1780 Gs [33].

In the centimetre-gram-second system, Oe and Gs are the classical units [34], which are used for the magnetic field intensity and magnetic induction intensity. For the saturation magnetization M_s of YIG, the unit of it is the same as magnetic induction intensity, whose unit should be Gs. However, the vacuum permeability is defined as the dimensionless quantity of 1 in the centimetre-gram-second system [35], leading to the numerical equivalence between Oe and Gs. So, to simplify the calculation of YIG, the unit of the M_s is often chosen as Oe [31], benefiting the unit unification in the calculation process.

When the EWs incident the medium of MP, the MP can be viewed as an anisotropic medium on dielectric constant, whose effective dielectric tensor is described as follows [30]:

$$\widehat{\boldsymbol{\varepsilon}}=\begin{bmatrix}\varepsilon_1 & 0 & \mathrm{j}\varepsilon_2\\ 0 & \varepsilon_3 & 0\\ -\mathrm{j}\varepsilon_2 & 0 & \varepsilon_1\end{bmatrix} \tag{3}$$

where

$$\varepsilon_1=1-\frac{\omega_p^2(\omega+j\nu)}{\omega[(\omega+j\nu)^2-\omega_c^2]} \tag{3-1}$$

$$\varepsilon_2=\frac{-\omega_p^2\omega_{\mathrm{c}}}{\omega[(\omega+j\nu)^2-\omega_c^2]} \tag{3-2}$$

$$\varepsilon_3=1-\frac{\omega_p^2}{\omega(\omega+j\nu)} \tag{3-3}$$

$$\varepsilon_{\mathrm{TE}}=\varepsilon_3 \tag{3-4}$$

$$\varepsilon_{\mathrm{TM}}=\frac{\varepsilon_1^2-\varepsilon_2^2}{\varepsilon_1} \tag{3-5}$$

where ω_p and ω_{c} are deemed as the plasma frequency, and the cyclotron frequency of electron [30], respectively, where $\omega_p=[(\mathrm{e}^2\mathrm{n_e})/(\varepsilon_0\mathrm{m})]^{1/2}$, and $\omega_{\mathrm{c}}=(\mathrm{e}B_O/\mathrm{m})$. Moreover, the $\mathrm{n_e}$, and ν are defined as the plasma density and collision frequency, where $\mathrm{n_e}=1\times10^{18}\ \mathrm{m}^{-}3$ [36], and ν is fixed as $\nu=0.0001\omega_{\mathrm{p}}$. For e, m, and ε_0, they represent the electric quantity, electric quality, and permittivity of the vacuum [30].

Given that the direction of E is along the $-y$-axis for the TE waves,$\boldsymbol{H}=-\sqrt{\frac{\varepsilon}{\mu}}\boldsymbol{E}$ can be used to calculate the magnitudes of the electric and magnetic fields for the TE waves. Then, the forms of the transfer matrices about A, B, C, and D are listed as follows [30,33]:

$$\mathrm{M}_a=\begin{bmatrix}\cos(k_{az}d_a) & \frac{j\sin(k_{az}d_a)}{\eta_a}\\ j\eta_a\sin(k_{az}d_a) & \cos(k_{az}d_a)\end{bmatrix} \tag{4-1}$$

$$\mathrm{M}_i=\begin{bmatrix}\cos(k_{iz}d_i)-\frac{k_{ix}\mu_{ik}}{k_{iz}\mu_{ir}}\sin(k_{iz}d_i) & j\eta_i\sin(k_{iz}d_i)\\ \frac{j}{\eta_i}[1+(\frac{k_{ix}\mu_{ik}}{k_{iz}\mu_{ir}})^2]\sin(k_{iz}d_i) & \cos(k_{iz}d_i)+\frac{k_{ix}\mu_{ik}}{k_{iz}\mu_{ir}}\sin(k_{iz}d_i)\end{bmatrix} \tag{4-2}$$

where a represents the media of A and B, and i stands for the media of C and D. Moreover, the k_{az}, k_{ix}, k_{iz}, η_a, and η_i can be attained from Refs. [30,33].

Considering the magnetic field of the TM waves is directed along the $+y$-axis, the magnitudes of the electric and magnetic fields for the TM waves can be calculated by $\boldsymbol{H}=\sqrt{\frac{\varepsilon}{\mu}}\boldsymbol{E}$. Then, the calculation methods of the transfer matrices are written as follows [30,33]:

$$\mathrm{M}_g=\begin{bmatrix}\cos(k_{gz}d_g) & \frac{-j\sin(k_{gz}d_g)}{\eta_g}\\ -j\eta_g\sin(k_{gz}d_g) & \cos(k_{gz}d_g)\end{bmatrix} \tag{5-1}$$

$$\mathrm{M}_q=\begin{bmatrix}\cos(k_{qz}d_q)+\frac{k_{qx}\varepsilon_{q2}}{k_{qz}\varepsilon_{q1}}\sin(k_{qz}d_q) & -\frac{j}{\eta_q}[1+(\frac{k_{qx}\varepsilon_{q2}}{k_{qz}\varepsilon_{q1}})^2]\sin(k_{qz}d_q)\\ -j\eta_q\sin(k_{qz}d_q) & \cos(k_{qz}d_q)-\frac{k_{qx}\varepsilon_{q2}}{k_{qz}\varepsilon_{q1}}\sin(k_{qz}d_q)\end{bmatrix} \tag{5-2}$$

where g is on behalf of the media of A, C, and D, and q is substituted by the medium of B. Furthermore, the equations of k_{gz}, k_{qx}, k_{qz}, η_g, and η_q can be calculated from Refs.[30,33].

Through the derivations of the above transfer matrices of A, B, C, and D, the transfer matrix of the proposed encoder can be demonstrated as follows [30,33]. For Structure 1, its entire transfer matrix can be described as:

$$\begin{aligned}\mathrm{M}_1&=(\mathrm{M_B}\mathrm{M_C})^2\mathrm{M_A}(\mathrm{M_C}\mathrm{M_B})^3\mathrm{M_A}(\mathrm{M_B}\mathrm{M_C})^2\\&=\begin{bmatrix}M_{11} & M_{12}\\ M_{21} & M_{22}\end{bmatrix}\end{aligned} \tag{6-1}$$

For Structure 2, its transfer matrix can be demonstrated as:

$$\begin{aligned}\mathrm{M}_2&=\mathrm{M_D}(\mathrm{M_B}\mathrm{M_C})^2\mathrm{M_A}(\mathrm{M_C}\mathrm{M_B})^3\mathrm{M_A}(\mathrm{M_B}\mathrm{M_C})^2\\&=\begin{bmatrix}M_{11} & M_{12}\\ M_{21} & M_{22}\end{bmatrix}\end{aligned} \tag{6-2}$$

The reflection coefficients about the given encoder can be written as the following [30,33]. For the TE waves, it can be deemed as:

$$r_{TE}=\frac{(M_{11}-\eta_0M_{12})\eta_0+(M_{21}-\eta_0M_{22})}{(M_{11}-\eta_0M_{12})\eta_0-(M_{21}-\eta_0M_{22})} \tag{7-1}$$

For the TM cases, its reflection coefficient can be indicated as:

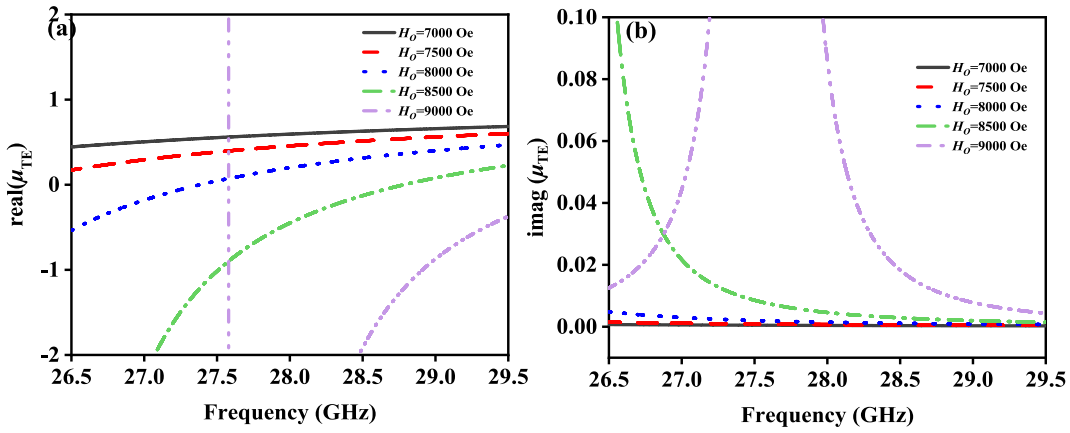

Fig. 2. **(a)** Relationship between the real part of μ_{TE} and H_O; **(b)** relationship between the imaginary part of μ_{TE} and H_O.

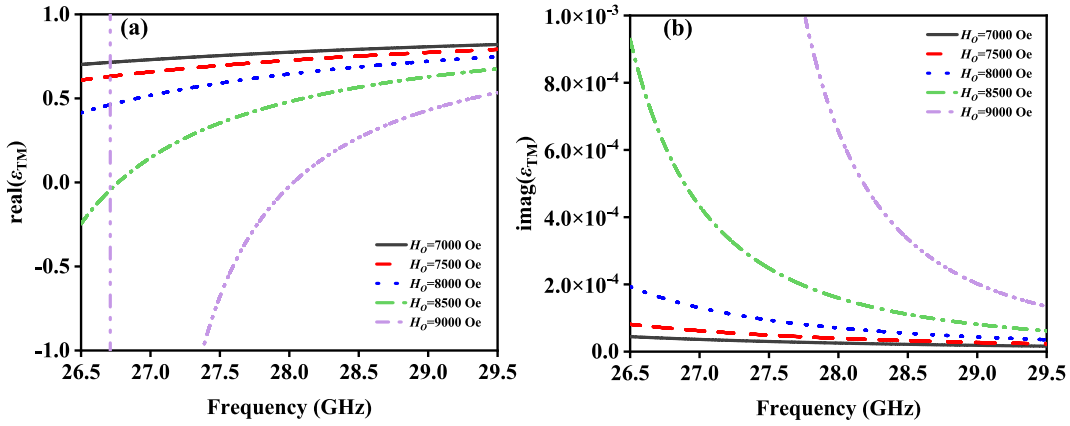

Fig. 3. **(a)** Influence of the H_O on the real part of ε_{TM}; **(b)** influence of the H_O on the imaginary part of ε_{TM}.

$$r_{TM} = \frac{(M_{11} + \eta_0 M_{12})\eta_0 - (M_{21} + \eta_0 M_{22})}{(M_{11} + \eta_0 M_{12})\eta_0 + (M_{21} + \eta_0 M_{22})} \tag{7-2}$$

The $r=|r|e^{j\varphi}$ is on behalf of the complicated reflection coefficient, whose φ stands for the phase of the reflected EWs [28]. Therefore, the reflectivities of the TE and TM waves can be deemed as $R_{TE}=|r_{TE}|^2$, and $R_{TM}=|r_{TM}|^2$. Moreover, φ_{TE} and φ_{TM} can be used to describe the phases of the TE and TM waves. To illustrate the PCs of EWs, accurately, it is non-negligible to calculate the axial ratio (*AR*) [37], whose formula is indicated as:

$$AR = \left(\frac{|R_{TE}|^2 + |R_{TM}|^2 + \sqrt{a}}{|R_{TE}|^2 + |R_{TM}|^2 - \sqrt{a}} \right)^{\frac{1}{2}} \tag{8}$$

where $a=|R_{TE}|^4+|R_{TM}|^4 + 2|R_{TE}|^2 \cdot |R_{TM}|^2 \cos(2\Delta\varphi)$, whose $\Delta\varphi$ is calculated as $\Delta\varphi = \varphi_{TM}\text{-}\varphi_{TE}$. The polarization forms are regulated by the amplitude and $\Delta\varphi$ of EWs. When the $\Delta\varphi$ meets $\Delta\varphi = 180^\circ \pm 180^\circ t$ ($t = 0$, 1, 2, 3…), the EWs are considered as LPWs [17]. If the EWs meet the needs of CPWs, their $\Delta\varphi$ must satisfy $\pm 90^\circ \pm 360^\circ t$($t = 0$, 1, 2, 3…), and *AR* is less than 3 dB [17]. For the CPWs, $\Delta\varphi = 90^\circ$ represents RHCPWs, and $\Delta\varphi$ = -90° denotes LHCPWs [17]. The EWs can be defined as elliptical polarization waves when the EWs do not meet the above needs of other polarization waves [17].

3. Analysis and discussion

Owing to the H_O tunability of the MP and YIG, the magnetic permeability of YIG and the dielectric constant of MP can be regulated to a certain extent by the H_O [30,31], which can be used for adjusting the phases of the TE and TM waves. For the MP and YIG, the H_O can only be applied to change the μ_{TE} of YIG and ε_{TM} of MP. Therefore, as shown in Fig. 2(a) and (b), if the frequency of EWs remains unchanged, with the H_O increasing from 7000 Oe to 8500 Oe at intervals of 500 Oe, the real part of μ_{TE} of YIG will reduce, while the imaginary part of μ_{TE} will elevate. When the H_O reaches 9000 Oe, the real and imaginary parts of μ_{TE} will mutate. Moreover, the real part and imaginary part of μ_{TE} are not very different in numerical terms, where the effect of the imaginary part of μ_{TE} can not be ignored. By adjusting the H_O, YIG can be changed to the mu-negative materials or mu-near-zero materials [38,39]. Also, the relationship between the H_O and ε_{TM} of MP can be displayed in Fig. 3 (a) and (b). As the H_O aggrandizes from 7000 Oe to 8500 Oe at intervals of 500 Oe, the real part and imaginary part of the ε_{TM} almost have a similar trend to those of the μ_{TE}. In addition, the real part of the ε_{TM} also has a mutation if the H_O approaches 9000 Oe. However, the real part of ε_{TM} is always smaller than 1 or even less than 0, and the imaginary part of ε_{TM} is almost equal to 0, where the MP can be considered as the epsilon-near-zero or epsilon-negative materials [38,39]. Hence, it is not ideal to employ the H_O to effectively alter the phases of the TE and TM waves for the given encoder, which is in favor of realizing the polarization encoding and CDs.

The thicknesses of A, B, C, and D are set as the above. The initial H_O is defined as 8730 Oe and the original θ is thought of as 56°. Since the proposed encoder is determined by the logic levels of the θ and MDL, it is decisive to discuss the effects of the θ and thickness of the MDL for the $\Delta\varphi$ between the TE and TM waves, which can be used to determine proper logic levels to fulfill the special PC in a special frequency range. Furthermore, due to the H_O making a certain difference in the $\Delta\varphi$ of the TE and TM waves, the H_O plays a crucial role in determining the

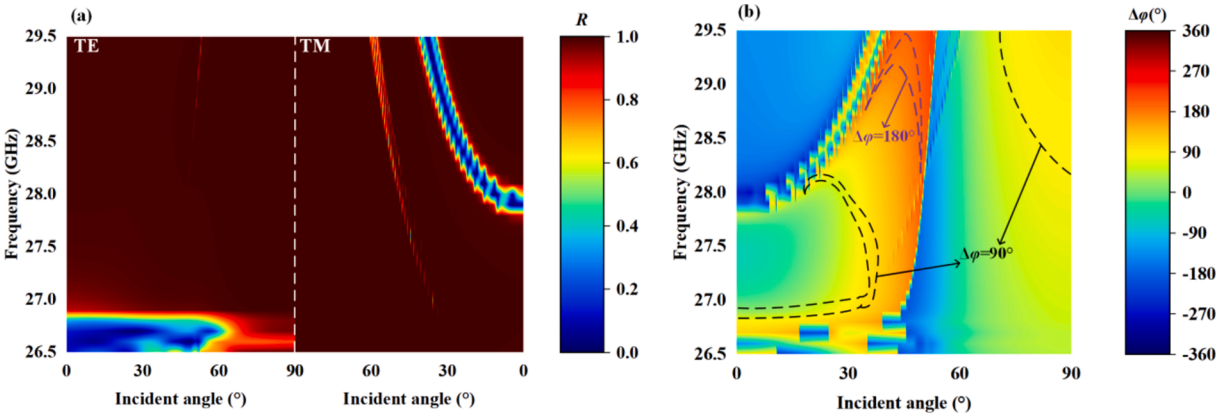

Fig. 4. **(a)** Influences of the θ on R under the TE and TM waves, with the θ varying from 0° to 90°; **(b)** the relationship between the θ and $\Delta\varphi$, where the θ is varied from 0° to 90°.

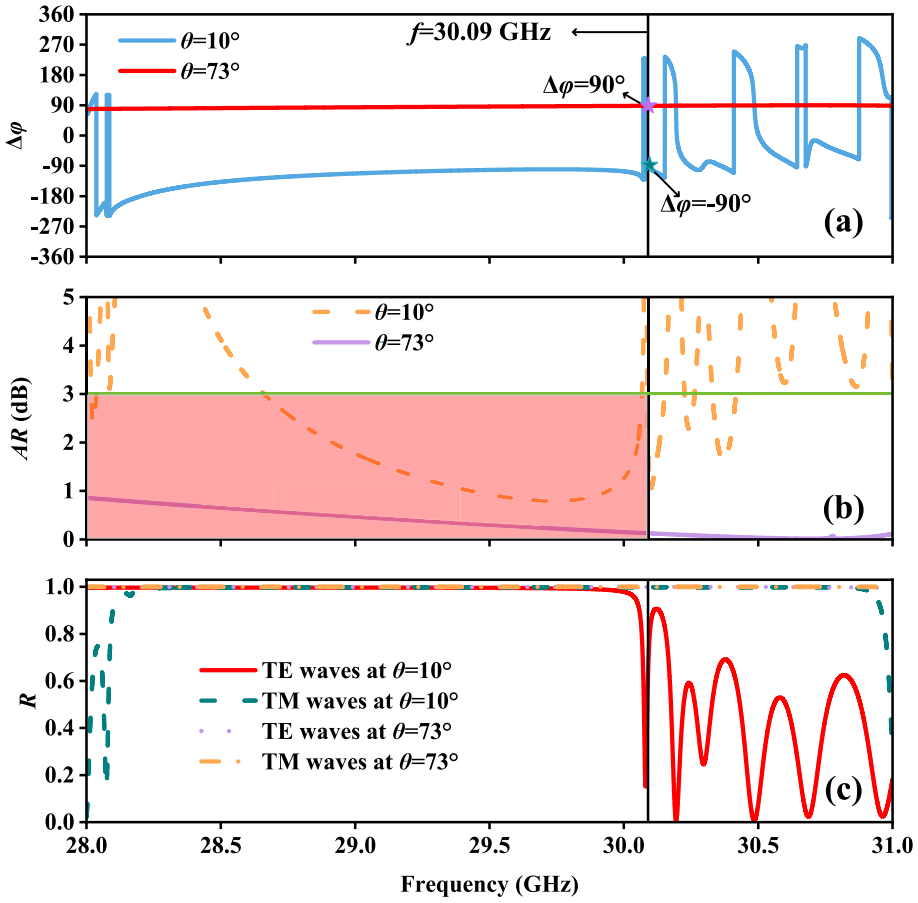

Fig. 5. **(a)** The $\Delta\varphi$ with the θ being 8° and 45°; **(b)** the AR when the θ keeps 8° and 45°; **(c)** the R of the TE and TM waves under the $\theta = 8°$ and $\theta = 46°$.

polarization forms of the reflected EWs. Therefore, the θ, H_O, and MDL will be discussed by fitting the corresponding three-dimensional graphs, which is useful to determine the proper logic levels corresponding to achieving certain PCs.

For the convenience of researching the relationship between the θ and PCs of EWs, the presented encoder is at the situation of Structure 1. The Eqs. (7-1), (7-2), and (8) for calculating the axial ratio and phase of EWs are given above. $\Delta\varphi = \varphi_{TM}$-$\varphi_{TE}$ stands for the phase difference between the TE and TM waves. Firstly, the three-dimensional diagrams of the R and $\Delta\varphi$ for the TE and TM waves are plotted in Fig. 4. As indicated in Fig. 4(a), when the θ is located in the range from 0° to 90°, the reflective frequency band of the TE and TM waves will appear, whose R is greater than 0.99. For the TE waves, the frequency of the reflective band almost covers the rough range of 27.0 GHz to 29.5 GHz, where the R is not affected by the θ except at individual frequency points. For the TM waves, their reflected frequency band remains stable, whose range is 26.5–29.5 GHz when the θ is at the about range of 60° to 90°. So, it is convenient to find the coincident reflection frequency bands for the TE and TM waves, meaning the TE and TM waves have similar amplitudes beneficial to satisfy the condition that the AR is less than 3 dB [40,41]. Then, by adjusting the proper $\Delta\varphi$, the special CPWs can be attained. As shown in Fig. 4(b), the $\Delta\varphi$ wrapped in black dotted lines is

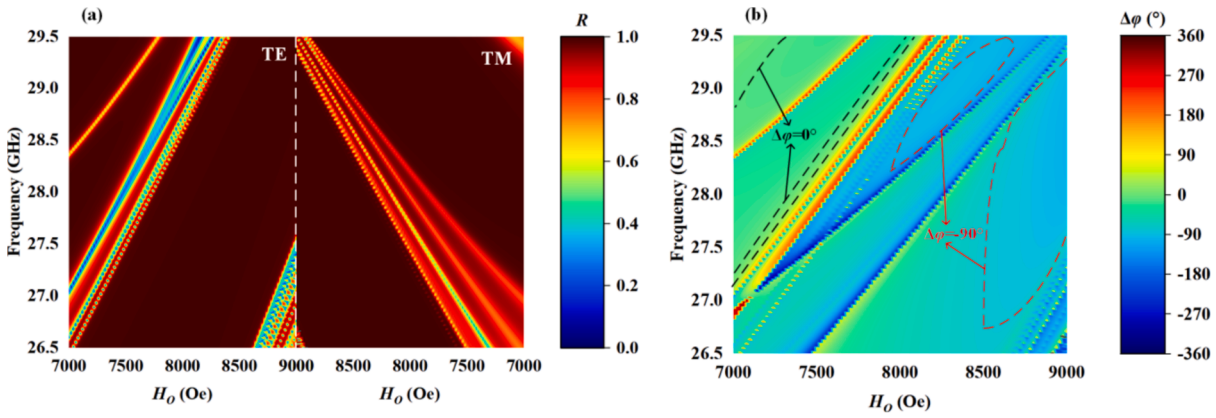

Fig. 6. **(a)** Influences of the H_O on the R under the TE and TM waves, with H_O shifting from 7000 Oe to 9000 Oe; **(b)** the relationship between the H_O and $\Delta\varphi$, where the H_O is altered from 7000 Oe to 9000 Oe.

about 90°, which means the EWs represent the RHCPWs when the *AR* is not more than 3 dB. Furthermore, the corresponding $\Delta\varphi = 180°$ satisfies the needs of LPWs, which is surrounded by modena dotted lines. In the above discussion, the θ plays a decisive role in realizing the certain PC in a certain frequency range, which is conducive to realizing the polarization encoding and CDs.

Through the above research about the effects of the θ on the R and $\Delta\varphi$, it is a handy and low-cost way to utilize the θ to attain the CD at a certain frequency, and the PC from LPWs to RHCPWs or other polarization waves in a special frequency band. Firstly, the $H_O = 8730$ Oe, and the presented configuration is Structure 1. When the frequency is at 30.09 GHz, as displayed in Fig. 5(a) and (b), when the $\theta = 10°$, the $\Delta\varphi$ = -90°, and *AR* is less than 3 dB, meaning the realization of converting LPWs to LHCPWs. However, when the θ converts from 10° to 73°, the conversion between the LPWs and RHCPWs can be fulfilled at 30.09 GHz, where the $\Delta\varphi$ is 90° (*AR* less than 3 dB). Meanwhile, in Fig. 5(c), the R of TE waves under the $\theta = 10°$ has distinct differences from one under the $\theta = 73°$, indicating the RHCPWs and LHCPWs outputs have different reflection characteristics and the CD can be effectively obtained. In addition, when the $\theta = 73°$, the polarization form of EWs is RHCPWs in the coverage of tangerine with the frequency range being 28.00 GHz ~ 30.09 GHz, while the range of the $\Delta\varphi$ and *AR*, covered by

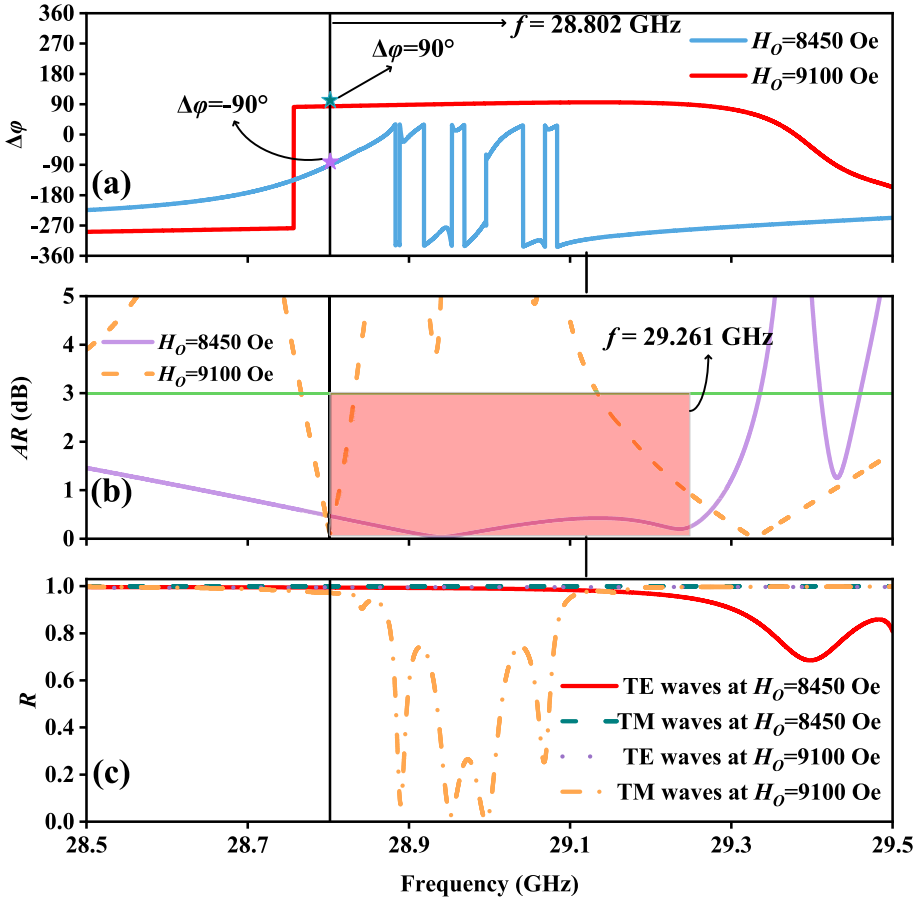

Fig. 7. **(a)** The $\Delta\varphi$ with the H_O being 8450 Oe and 9100 Oe; **(b)** the *AR* when the H_O keeps 8450 Oe and 9100 Oe; **(c)** the R of the TE and TM waves under the H_O = 8450 Oe and H_O = 9100 Oe.

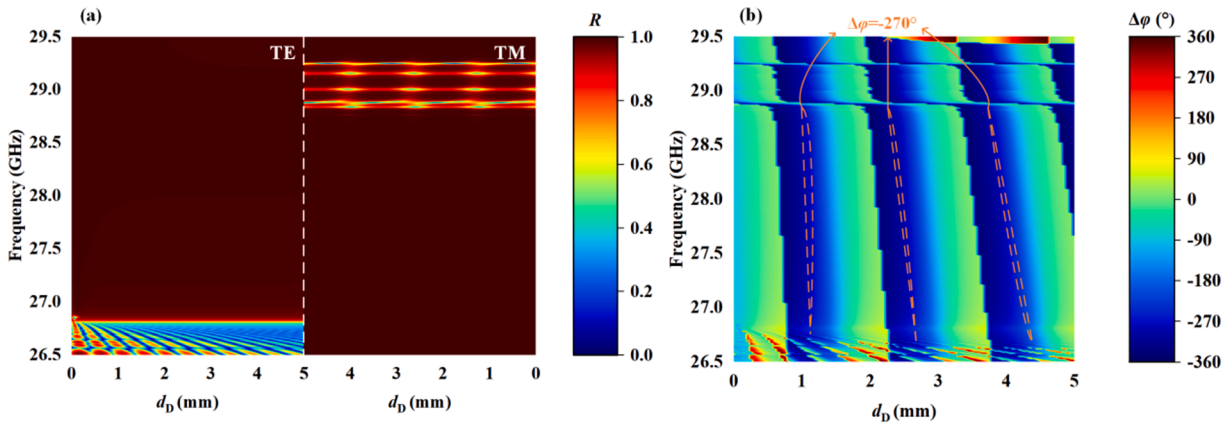

Fig. 8. **(a)** Influences of the d_D on the R under the TE and TM waves, with the thickness of the MDL changing from 0 mm to 5 mm; **(b)** the relationship between the d_D and $\Delta\varphi$, where the d_D is shifted from 0 mm to 5 mm.

tangerine, can not concurrently meet the demands of CPWs when the θ is shifted to 10°. Hence, the designed encoder can effectively obtain the Functions of the CD and PC from LPWs to RHCPWs or other polarization waves at the same time with the variation of θ.

The configuration of the given encoder still keeps Structure 1, and the θ is fixed at 56°. As plotted in Fig. 6(a), with the H_O changing from 7000 Oe to 9000 Oe, the TE and TM waves will own broad reflected frequency bands, whose R are not less than 0.99. As the H_O increases from 7000 Oe to 9000 Oe, the main frequency band of reflection under TE waves begins to increase to the maximum, ranging from 26.5–29.5 GHz, and then decreases to the coverage of 27.5–29.5 GHz. For TM waves, their reflective frequency bands are divided into two main parts, whose bandwidths have opposite trends with the H_O increasing from 7000 Oe to 9000 Oe. So, it is easy to find the overlapping frequency bands of reflection, which can be employed to attain a stable and broad frequency band of AR less than 3 dB [40,41]. Moreover, the H_O is useful to alter the $\Delta\varphi$ to some degrees, which is implied in Fig. 6(b). With the H_O increasing from 7000 Oe to 9000 Oe, the $\Delta\varphi$ will change to a certain extent, whose range is roughly from −270° to 323°. The $\Delta\varphi$ is most focused on −90° to 0°, where the $\Delta\varphi = -90°$ is encircled by red dashed lines. Therefore, when the AR is less than 3 dB, the $\Delta\varphi$ can be adjusted by the H_O to realize the conversions from LPWs to LHCPWs. Furthermore, the $\Delta\varphi = 0°$, covered by black dashed lines, meaning the polarization form of EWs is LPWs. Therefore, choosing a proper H_O is beneficial to the realization of a certain PC.

When the magnetization of YIG reaches saturation, all magnetic dipoles in YIG will be directed with the applied magnetic field. If the magnetization is lower than M_s, The loss of YIG is large and the radio frequency interaction is weakened. So, the magnetization of YIG is always assumed in a saturated state to ensure the normal working of YIG [42]. More importantly, when the magnetization reaches saturation, the value of it will not be changed by the increase of the H_O. Hence, the high H_O is mainly employed in adjusting the resonance frequency and does not affect the M_s and the circular frequency in YIG [33].

For the realization of the applied magnetic field, the gradient magnetic field is an ideal way. Firstly, a magnetic material must be positioned in a loop and an electric current is added to the coil. The energized coil generates a magnetic field, which magnetizes the magnetic material, which in turn generates a magnetic field. When gradient magnetic field coils are used, a spatial linear magnetic field can be generated, and it can be found experimentally and theoretically in Ref. [43]. Moreover, the spatial linear magnetic field can be adjusted to reach the demanded value, including the high magnetic field [44]. Given that the realization conditions of the gradient magnetic field are not very harsh, the way can be utilized as the magnetic field source for the designed encoder with a small size.

As the H_O can be changed, the μ_{TE} of YIG can be adjusted to alter the $\Delta\varphi$ and AR of EWs, which can be applied to achieve certain PCs and CDs. Structure 2 is chosen, and θ is fixed as 17°. As presented in Fig. 7(a) and (b), when the $H_O = 8450$ Oe and frequency of EWs is 28.802 GHz, the conversion between LPWs and LHCPWs can be attained, with the $\Delta\varphi$ being −90°, and AR less than 3 dB. When the H_O is switched from 8450 Oe to 9100 Oe, the LPWs can convert to RHCPWs at 28.802 GHz with the $\Delta\varphi$ being 90°, and AR smaller than 3 dB. However, in Fig. 7(c), under TE waves, the R of $H_O = 8450$ Oe is equal to the one of $H_O = 9100$ Oe while the R of $H_O = 8450$ Oe under TM waves has an obvious difference from the one of $H_O = 9100$ Oe under TM waves. The result shows the reflection characteristics of LHCPWs output are different from the ones of RHCPWs output, meaning the CD at 28.802 GHz can be realized. Moreover, in the range of 28.802 GHz–29.261 GHz covered by tangerine, the EWs can not satisfy the demands of CPWs with the bandwidth of 0.495 GHz when the H_O is 8450 Oe. With the H_O switching from 8450 Oe to 9100 Oe, in the coverage of tangerine, the PC from LPWs to RHCPWs can be attained in the range of 28.802 GHz–29.261 GHz. Hence, it is convenient and accurate to achieve the CD and PCs from LPWs to RHCPWs or other polarization waves for the proposed encoder by changing the H_O.

Owning the tunability of H_O, YIG is a classical material and has a wide range of applications, where the thicknesses of these typical YIG-based experimental devices often reach mm, μm, and nm [45–47]. Owing to that the proposed encoder is working at GHz, the thicknesses of the dielectric media A, B, C, and D need to reach mm or cm, which are supposed to be similar to the wavelength of the working EWs. Hence, the values of the d_A, d_B, d_C, and d_D are reasonable.

The presented encoder can be converted from Structure 1 to Structure 2 when the special MDL is added in the previous term of Structure 1. The value of θ is considered as 56°, and the H_O is set as 8730 Oe. Thinking that the MDL can be used as the logic levels for the special PCs, the d_D of the MDL can play an indispensable role in researching the AR and $\Delta\varphi$. As demonstrated in Fig. 8(a), when the d_D is in the range from 0 mm to 5 mm, The R of the TE waves are greater than 0.99 in the frequency range from 26.9 GHz to 29.5 GHz. For TM waves, with the d_D changing from 0 mm to 5 mm, their reflective frequency band remains stable within the frequency coverage from 26.5 GHz to 28.7 GHz. Therefore, it is handy to attain an overlapping frequency band of the R, greater than 0.99, under the TE and TM waves, which can make sure the amplitudes of the TE and TM waves are closer [40,41]. In addition, the effect of the d_D on the $\Delta\varphi$ is demonstrated in Fig. 8(b). If the AR is less than 3 dB, the $\Delta\varphi = -270°$, surrounded by the orange dotted lines, indicates the EWs are on behalf of the RHCPWs. Through the addition of the MDL with a proper d_D, it is convenient to ensure the amplitudes of the TE and TM waves are closer, which is beneficial to attain CPWs within a wide frequency band. Hence, the MDL with a unique thickness can be defined as logic levels to find the proper $\Delta\varphi$ and AR, meeting the

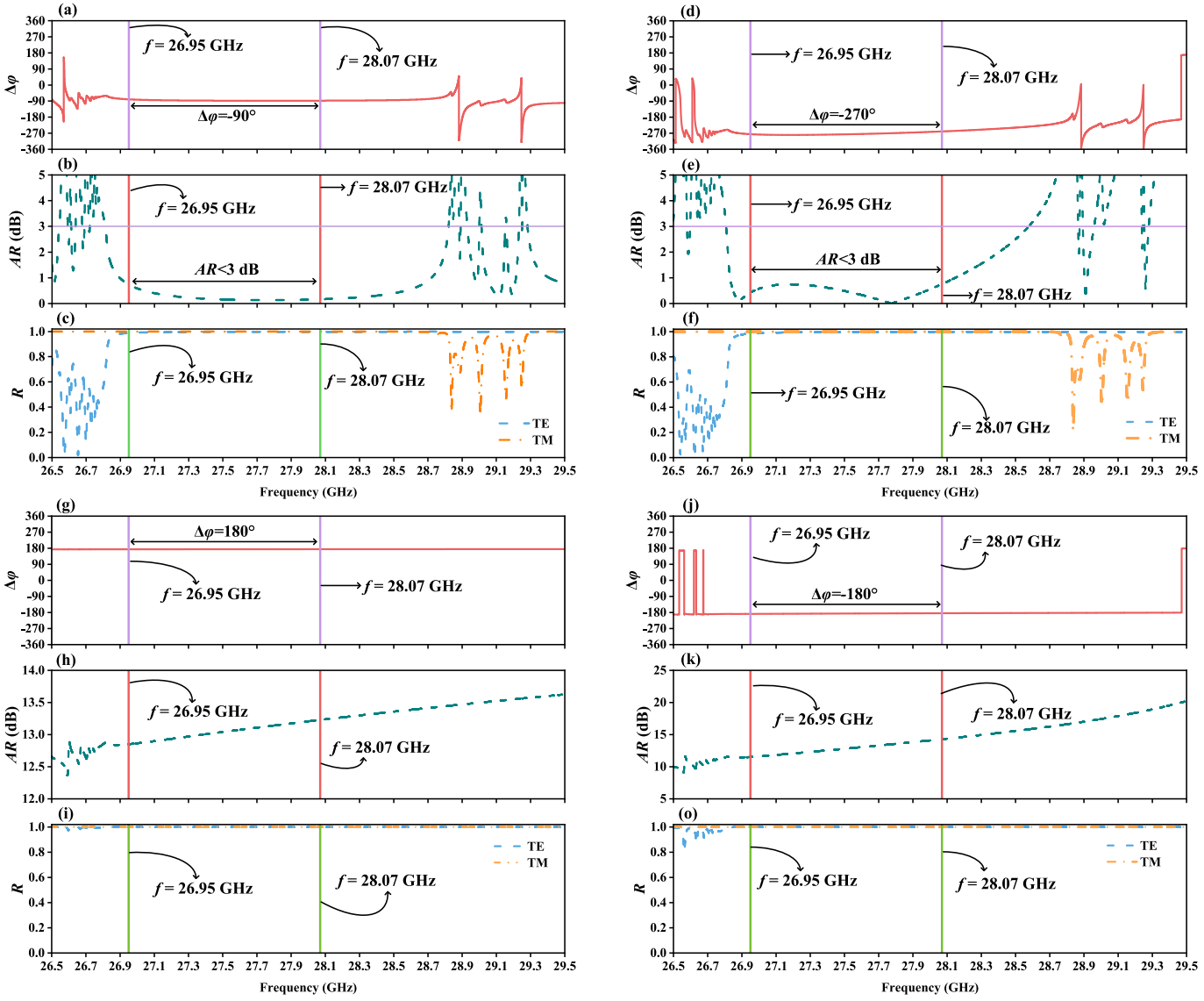

Fig. 9. **(a)** The $\Delta\varphi$ with the logic code being "10"; **(b)** the *AR* when the logic code is "10"; **(c)** the *R* of the TE and TM waves, whose logic code is "10"; **(d)** the $\Delta\varphi$ with the logic code being "11"; **(e)** the *AR* when the logic code is "11"; **(f)** the *R* of the TE and TM waves, whose logic code is "11"; **(g)** the $\Delta\varphi$, with the logic code being "00"; **(h)** the *AR* when the logic code is "00"; **(i)** the *R* of the TE and TM waves, whose logic code is "00"; **(j)** the $\Delta\varphi$, with the logic code being "01"; **(k)** the *AR* when the logic code is "01"; **(o)** the *R* of the TE and TM waves, whose logic code is "01".

needs of CPWs.

Through the above discussions about the θ, H_O, and d_D, the $\theta_1 = 56°$, and $\theta_2 = 89°$ can be defined as the logic level "1″, and logic level "0", respectively, which are specified as the first input. For the MDL, the d_D is fixed at 2.59 mm. In addition, the logic levels "1", and "0" are denoted as the addition and absence of the MDL, severally, which are defined as the second inputs. For the improvement of the $\Delta\varphi$, the H_O will be set as 8730 Oe. The effects of the combinations of the logic codes on the PCs will be studied.

The controllable PC and CPWs separation are of great importance, where the PCs can be elected by controlling the logic inputs, accurately and conveniently. The proposed encoder can be tuned by the θ and MDL to realize the specific polarization outputs. When the logic code is "10" with the θ being 56°, and the MDL being absent, as shown in Fig. 9(a)-(c), the conversion from LPWs to LHCPWs can be realized in the frequency range of 26.95 GHz–28.07 GHz, whose $\Delta\varphi$ is −90°, and *AR* is less than 3 dB. The bandwidth is 1.12 GHz. When the $\theta = 56°$ and the MDL is added, meaning the logic code switches to "11", as indicated in Fig. 9(d)-(f), the $\Delta\varphi$ = -270° and *AR* keeps smaller than 3 dB in the range of 26.95 GHz–28.07 GHz, indicating the polarization form meets the RHCPWs with the bandwidth of 1.12 GHz. If the θ is altered to 89° and the MDL is absent, the logic code shifts to "00". The concrete $\Delta\varphi$ and *AR* are displayed in Fig. 9(g)-(i). In the range of 26.95 GHZ–28.07 GHz, the $\Delta\varphi$ keeps 180° and the *AR* is all bigger than 10 dB, where the polarization form switches smoothly to LPWs. When the logic code is "01", the θ = 89°, and the MDL is added, in Fig. 9(j), the $\Delta\varphi$ keeps −180° from 26.95 GHz to 28.07 GHz. Moreover, the *AR* is always keeping more than 10 dB in Fig. 9(k). Therefore, the polarization form greatly meets the LPWs when the logic code keeps "01". Through the above combinations

Table 1
The relationship between the logic codes and the polarization outputs.

The incident angle	The MDL	The logic code	The form of polarization output
1 (θ_1)	0 (absence)	10	LHCPWs
1 (θ_1)	1 (addition)	11	RHCPWs
0 (θ_2)	0 (absence)	01	LPWs
0 (θ_2)	1 (addition)	00	LPWs

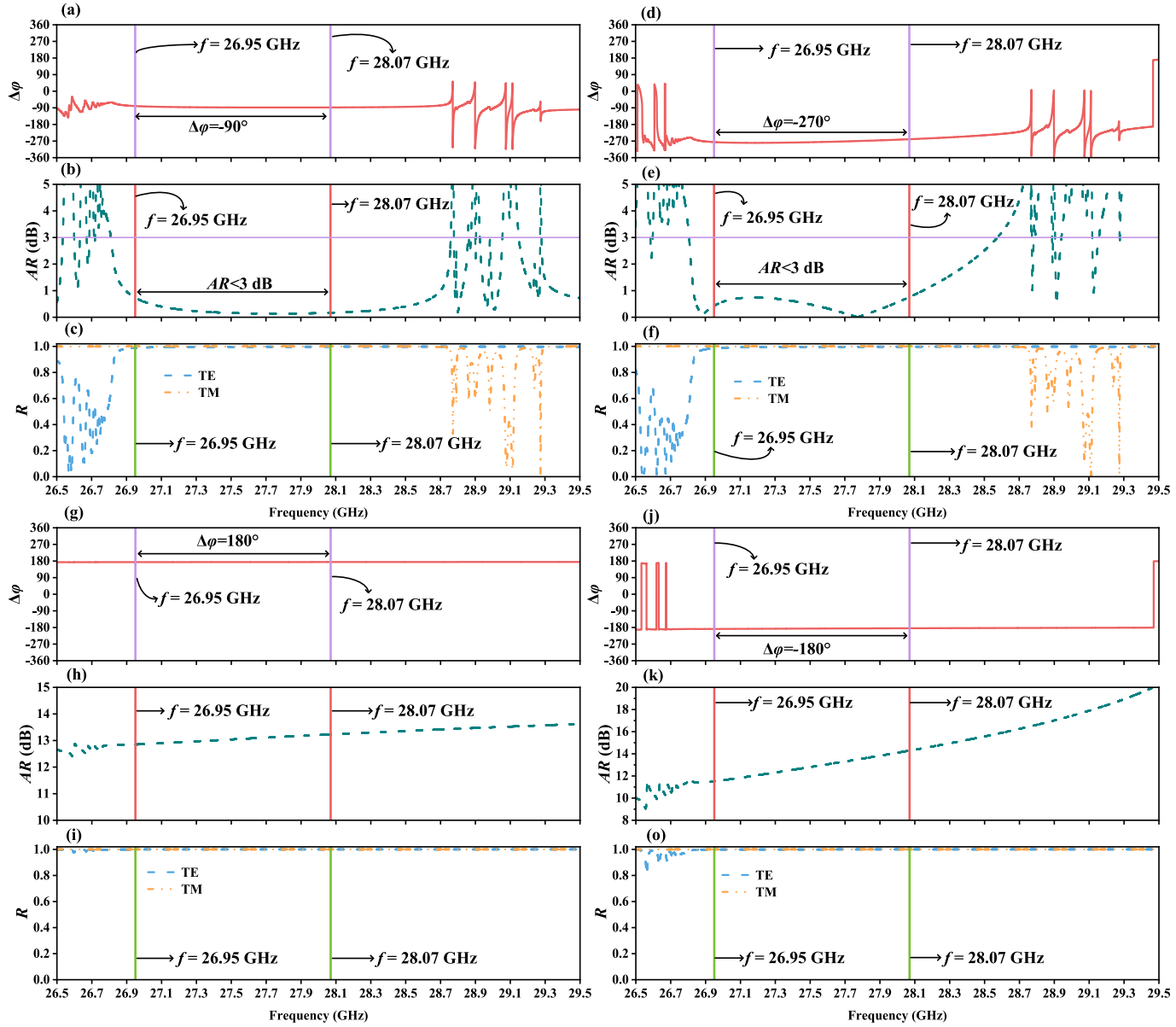

Fig.10. the periodic number of (BC) is 4 in Structure 1 and 2. **(a)** The $\Delta\varphi$ with the logic code being "10"; **(b)** the *AR* when the logic code is "10"; **(c)** the *R* of the TE and TM waves, whose logic code is "10"; **(d)** the $\Delta\varphi$ with the logic code being "11"; **(e)** the *AR* when the logic code is "11"; **(f)** the *R* of the TE and TM waves, whose logic code is "11"; **(g)** the $\Delta\varphi$, with the logic code being "00"; **(h)** the *AR* when the logic code is "00"; **(i)** the *R* of the TE and TM waves, whose logic code is "00"; **(j)** the $\Delta\varphi$, with the logic code being "01"; **(k)** the *AR* when the logic code is "01"; **(o)** the *R* of the TE and TM waves, whose logic code is "01".

between the logic inputs and the certain polarization outputs, the proposed encoder can realize the polarization outputs of LPWs, RHCPWs, and LHCPWs in the frequency range of 26.95 GHz–28.07 GHz, which not only has higher application possibility and value in practical application but also can be considered as an excellent idea to attain the needed polarization outputs with the accurate logic inputs. To explain the specific states of logic codes more evidently, Table 1 will demonstrate the relationship between the logic codes and the polarization forms. The results indicate the proposed encoder is capable of achieving the polarization output by the special logic codes, accurately and handily.

For the above discussion of polarization encoding, the encoder is always in Structure 1 or Structure 2, where Structure 1 represents $\{(BC)^2A(CB)^3A(BC)^2\}$, and Structure 2 stands for $\{D(BC)^2A(CB)^3A(BC)^2\}$. Therefore, considering the structures of the given encoder own low numbers of layers, it is necessary to research the impacts of the addition of layer numbers on the polarization encoding. Here, the periods of (BC) in Structure 1 and 2 are increased from 2 to 4 to study the possibility of polarization encoding. As indicated in Fig. 10(a)-(c), when the θ is fixed as 56°, and the MDL is the absence, the conversion from LPWs to LHCPWs can be attained in 26.95 GHz-28.07 GHz, with $\Delta\varphi$ and *AR* being −90° and smaller than 3 dB in the bandwidth of 1.12 GHz. So, the logic code "10" can be got. If the θ keeps 56°, and the MDL is added, Fig. 10(d)-(f) show the $\Delta\varphi$ = -270° and *AR* keep less than 3 dB in the range of 26.95 GHz-28.07 GHz, meaning the RHCPWs can be obtained and the logic code "11" is viable. Through converting θ from 56° to 89° and removing the MDL, as shown in Fig. 10(g)-(i), the $\Delta\varphi$ remains 180°, and the *AR* is always keeping higher than 10 dB from 26.95 GHz to 28.07 GHz, revealing the reflected EWs is LPWs. As a result, the logic code "00" can be fulfilled. With the $\theta = 89°$ and MDL being added, in the coverage of 26.95 GHz-28.07 GHz, the $\Delta\varphi$ is −180°, and *AR* remains larger than 10 dB, which are displayed in Fig. 10(j)-(o). Hence, the conditions of LPWs can be satisfied, indicating the success of the logic code "01". Although the periods of (BC) in Structure 1 and Structure 2 are increased from 2 to 4, the polarization encoding can be realized

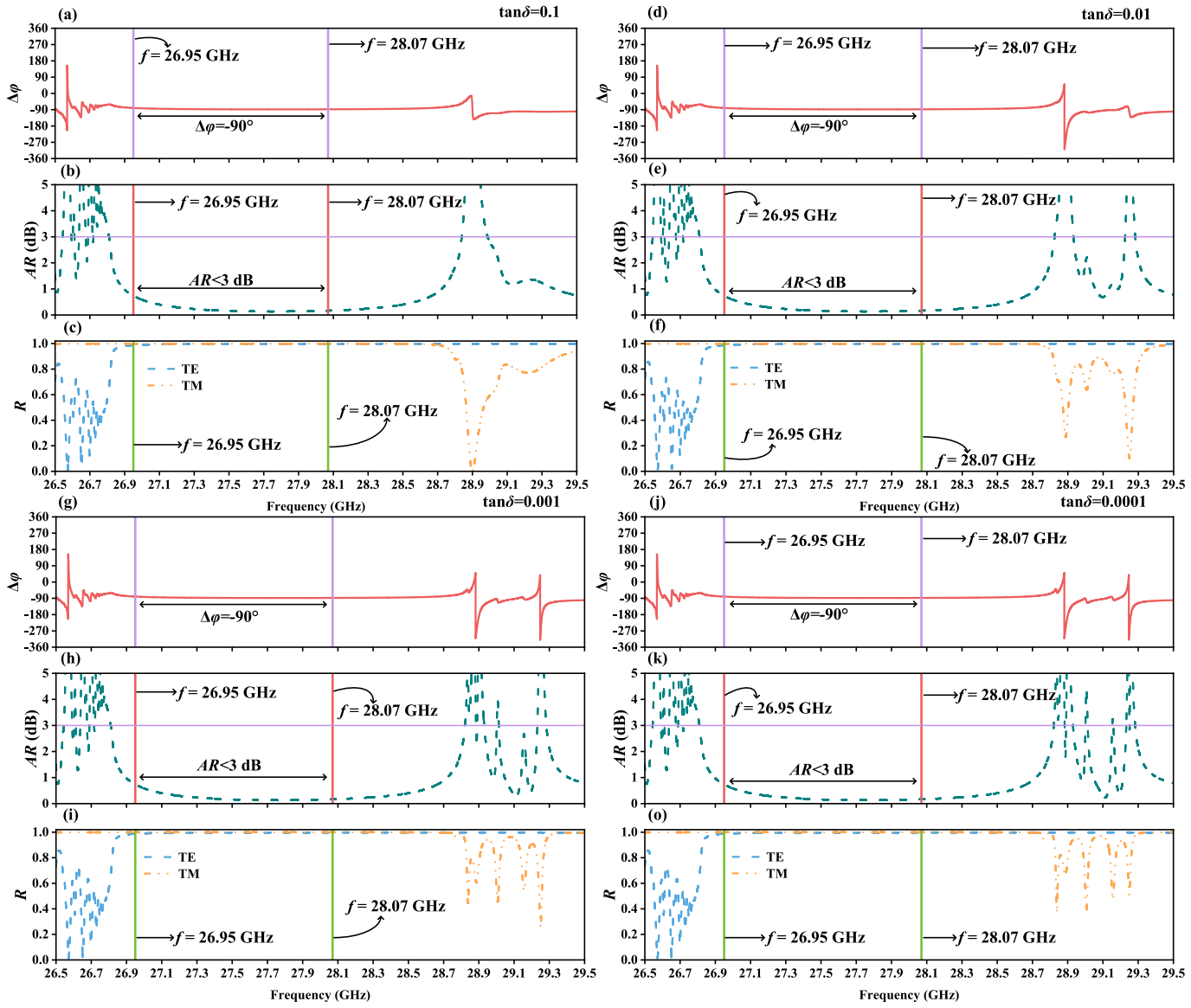

Fig.11. the encoder is at the situation of the logic code "10". **(a)** the $\Delta\varphi$, with the $\tan\delta = 0.1$; **(b)** the *AR* when the $\tan\delta$ is equal to 0.1; **(c)** the *R* of TE and TM waves, whose $\tan\delta$ is 0.1; **(d)** the $\Delta\varphi$ with the $\tan\delta = 0.01$; **(e)** the *AR* when the $\tan\delta$ is 0.01; **(f)** the *R* of the TE and TM waves, whose $\tan\delta$ is 0.01; **(g)** the $\Delta\varphi$, with the $\tan\delta$ being 0.001; **(h)** the *AR* when the $\tan\delta$ is 0.001; **(i)** the *R* of the TE and TM waves, whose $\tan\delta$ is 0.001; **(j)** the $\Delta\varphi$, with the $\tan\delta$ being 0.0001; **(k)** the *AR* when the $\tan\delta$ is 0.0001; **(o)** the *R* of the TE and TM waves, whose $\tan\delta$ is 0.0001.

successfully with the same conditions and frequency range, which can prove the period numbers of (BC) have a small influence on the encoding performance of the designed encoder.

The modulation of the proposed encoder focuses on reflected EWs. So, it is meaningful to take the influence of the penetration depth of the EWs source on PC into account. Here, given that both the dielectric constant of MP and the magnetic permeability of YIG involve imaginary parts, the effect of the loss tangent angle of the common dielectric A should be researched to ensure the stability of the given encoder. Firstly, the loss tangent angle of A is defined as $\tan\delta$, whose values are assumed

Table 2
The comparisons between the past encoders and the designed encoder.

Refs.	Bandwidth	Single frequency point	Polarization coding	Function
[1]	×	√	√	LPWs convert to CPWs
[11]	√	×	×	A multivalued logic circuit bated on optical shadow casting
[14]	×	√	×	A multilayer porous silicon with multiple bit encodings
[15]	√	×	×	The information encryption using the phase transition characteristics of vanadium dioxide
[16]	×	√	√	LPWs convert to CPWs and EPWs EPWs convert to LPWs and CPWs
[17]	×	√	√	LPWs convert LPWs, CPWs, and EPWs
[48]	×	√	×	The microbeads with color information coding
[49]	√	×	×	Polychromatic dual-mode imaging
This work	√	×	√	LPWs convert to LPWs or CPWs

as 0.1, 0.01, 0.001, and 0.0001. To make the discussion convenient, the situation of the logic code "10" is chosen as the instance, which is detailedly illustrated in Fig. 9(a)-(c). When the tanδ of A is fixed as 0.1, as revealed in Fig. 11(a)-(c), the $\Delta\varphi$ = -90°, and the *AR* is always less than 3 dB in the range of 26.95 GHz to 28.07 GHz, where the conversion from LPWs to LHCPWs can be fulfilled. If the tanδ is converted to 0.01, as revealed in Fig. 11(d)-(f), the PC from LPWs to LHCPWs can be fulfilled from 26.95 GHz to 28.07 GHz, whose $\Delta\varphi$ and *AR* are −90° and smaller than 3 dB. With the tanδ being 0.001, the $\Delta\varphi$ is equal to −90° and *AR* remains less than 3 dB in the range of 26.95 GHz-28.07 GHz, which are indicated in Fig. 11(g)-(i). Therefore, the reflected EWs meet the conditions of LHCPWs. Finally, As the tanδ shifts to 0.0001, the LPWs can be converted to LHCPWs within the coverage of 26.95 GHz-28.07 GHz, displayed in Fig. 11(j)-(o), whose $\Delta\varphi$ = -90° and *AR* is not higher than 3 dB. Hence, compared with the situation of A without tanδ, the *AR* and *R* are all obviously affected by the tanδ of A. Fortunately, the frequency band used for polarization encoding remains stable. So, when the influence of the penetration depth is considered, the ideal polarization encoding can be fulfilled by the encoder without any changes in the working conditions.

Finally, although the encoders have experienced rapid development, most encoders are mainly limited to electromagnetic propagation information imaging, and a few are focused on PC at a single frequency point. To visually and conveniently describe the advantages of the polarization encode presented, Table 2 sums up the past research about encoders, and compares them with the proposed encoder. The results of the Table 2 or demonstrates that the designed encoder in this paper not only has the CDs and polarization encoding within a specific bandwidth but also is beneficial to precise manipulation of PC and application possibility.

4. Conclusions

To sum up, the CD and polarization encoding, controlled by the θ, H_O, and MDL, are researched in this paper. With the excellent combinations between MP and YIG, the designed encoder has the ability to adjust the CDs and polarization encoding by electing the proper θ, H_O, and d_D. Through discussing the effects of the θ, H_O, and MDL on the $\Delta\varphi$ and *R*, the CDs can be fulfilled at a certain point by controlling the θ, H_O, and MDL, where PCs from LPWs to RHCPWs or other polarization waves can be obtained within the special bandwidth at the same time. More importantly, with the two different values of the θ and MDL being defined as four different input logic levels, the polarization outputs of the LPWs, RHCPWs, and LHCPWs can be preciously controlled in the same frequency range. Therefore, by connecting the four logic levels with the corresponding output forms of polarization, the function of polarization encoding can be realized. The designed encoder can realize the precise control of the polarization outputs by a handy method of changing the θ, H_O, and MDL, whose specific functions are mainly focused on certain bandwidths. Therefore, the design idea not only provides an effective approach to fulfill selective polarized outputs with low cost, no pollution, convenient operation, and real-time monitoring but also owns a higher practical application possibility and value.

CRediT authorship contribution statement

Chuan-Qi Wu: Writing – original draft, Investigation, Formal analysis, Data curation. **Jun-Yang Sui:** Validation, Software, Resources, Methodology. **Qi Chen:** Visualization, Validation, Data curation. **Xing-Zhou Tang:** Writing – review & editing, Funding acquisition. **Hai-Feng Zhang:** Writing – review & editing, Supervision, Conceptualization.

Declaration of competing interest

The authors declare that they have no known competing financial interests or personal relationships that could have appeared to influence the work reported in this paper.

Acknowledgement

The work is supported by the National Key Research and Development Program of China (No. 2022YFA1405000), the National Natural Science Foundation of China (No. 62375141), the Natural Science Foundation of Jiangsu Province, Major Project (No. BK20243067).

Data availability

Data will be made available on request.

References

[1] Y. Jing, Y. Li, J. Zhang, J. Wang, M. Feng, T. Qiu, S. Qu, Achieving circular-to-linear polarization conversion and beam deflection simultaneously using anisotropic coding metasurfaces, Sci. Rep. 9 (2019) 12264.
[2] I. Naito, A note on representation of electromagnetic plane wave polarization state, IEEE Trans. Antennas Propag. 70 (2022) 6066–6071.
[3] J. Qiao, G. Feng, G. Yao, C. Li, Y. Tang, B. Fang, T. Zhao, Z. Hong, X. Jing, Research progress on the principle and application of multi-dimensional information encryption based on metasurface, Opt. Laser Technol. 179 (2024) 111263.
[4] G. Ozturk, U.C. Hasar, M. Ertugrul, F. Tutar, M.F. Corapsiz, M. Kurt, M.S. Alfaqawi, An efficient cost effective wide-angle metasurface-based linear and circular polarization converter for X-, Ku-and K-band applications, Opt. Laser Technol. 163 (2023) 109404.
[5] Z. Pan, Z. Zhou, Z. Song, Terahertz generations of transmissive deflection, focusing, and orbital angular momentum with polarization conversion, Opt. Laser Technol. 159 (2023) 109036.
[6] S. Yan, G.A. Vandenbosch, Compact circular polarizer based on chiral twisted double split-ring resonator, Appl. Phys. Lett. 102 (2013) 103503.
[7] M. Mutlu, A.E. Akosman, E. Ozbay, Broadband circular polarizer based on high-contrast gratings, Opt. Lett. 37 (2012) 2094–2096.
[8] Y. Sun, Y. Liu, T. Wu, Y. Wang, J. Li, H. Ye, X. Wang, All-dielectric metasurface for linear-polarization conversion with an arbitrary polarization rotating angle, Opt. Laser Technol. 157 (2023) 108762.
[9] Y. Zhang, W. Luan, X. Yan, X. Gao, S. Zhang, Z. Jing, J. Yao, Dual-directional broadband linear-to-linear polarization conversion using multi-layer metamaterials, Plasmonics 17 (2022) 1411–1418.
[10] B. Murmann, Digitally assisted analog circuits, IEEE Micro 26 (2006) 38–47.
[11] M.S. Alam, M.A. Karim, Multiple-valued logic unit design using polarization-encoded optical shadow-casting, Opt. Laser Technol. 25 (1993) 17–23.
[12] I.F. Akyildiz, Wireless sensor networks: a survey, Computer Netw. 2 (2002) 6–14.
[13] G. Böcherer, S. Patrick, S. Fabian, Probabilistic shaping and forward error correction for fiber-optic communication systems, J. Lightwave Technol. 37 (2019) 230–244.
[14] J. Park, S. Cho, H. Sohn, Y.C. Ko, Multiple bit encodings of multilayer porous silicon, J. Korean Phys. Soc. 50 (2007) 695.
[15] J. Wang, M. Wang, Q. Xie, W. Li, L. Zhang, L. Zhang, P. Zhou, Multilevel information encryption mediated by reconfigurable thermal emission in smart bilayer material, Laser Photonics Rev. 18 (2024) 2301106.
[16] J. Li, P. Yu, H. Cheng, W. Liu, Z. Li, B. Xie, J. Tian, Optical polarization encoding using graphene-loaded plasmonic metasurfaces, Adv. Opt. Mater. 4 (2016) 91–98.
[17] S. Rao, Y. Zhou, B.F. Wan, H.F. Zhang, Tunable polarization encoder capable of polarization conversion and separation based on a layered photonic structure, IEEE J. Selected Top. Quantum Electron.: Nonlinear Integrated Photonics 29 (2022) 1–8.
[18] M.M. Hamarsheh, M.K. Abduullah, S. Khatun, H.M. Shalaby, Fast frequency modulation optical code division multiple access communication system, Opt Laser Technol. 39 (2007) 605–609.
[19] S. Fang, Z. Yang, Y. Tao, W. Lv, J. Jiang, D.Q. Zhang, F.Z. Shu, Design and experimental realization of triple-band filtering metamaterial in sub-terahertz band enabled by conductivity coupling response of two identical split rings, Opt. Laser Technol. 183 (2025) 112345.
[20] H. Xiong, X. Ma, H. Liu, D. Xiao, H. Zhang, Research on electromagnetic energy absorption and conversion device with four-ring multi-resistance structure, Appl. Phys. Lett. 123 (2023).
[21] Q. Yang, H. Xiong, J.H. Deng, B.X. Wang, W.X. Peng, H.Q. Zhang, Polarization-insensitive composite gradient-index metasurface array for microwave power reception, Appl. Phys. Lett. 122 (2023).
[22] H. Xiong, Q. Yang, Y.Z. Huang, J.H. Deng, B.X. Wang, H.Q. Zhang, High-efficiency microwave wireless power transmission via reflective phase gradient metasurfaces and surface wave aggregation, Acs Appl. Mater. Interfaces 16 (2024) 60189–60196.
[23] H. Xiong, J.Y. Xie, Y.J. Liu, B.X. Wang, D.P. Xiao, H.Q. Zhang, Microwave hyperthermia technology based on near-field focused metasurfaces: design and implementation, Adv. Funct. Mater. (2024).
[24] J. Zhang, Y. Ruan, Z.D. Hu, J. Wu, J. Wang, An enhanced high Q-factor resonance of quasi-bound states in the continuum with all-dielectric metasurface based on multilayer film structures, Ieee Sens. J. 23 (2023) 2070–2075.

[25] Y. Ren, T. Zhou, C. Jiang, B. Tang, Thermally switching between perfect absorber and asymmetric transmission in vanadium dioxide-assisted metamaterials, Opt. Express. 29 (2021) 7666–7679.
[26] A. Habashi, C. Ghobadi, J. Nourinia, R. Naderali, A bi-Layered chiral metasurface as a multi-functional polarization convertor with high incidence angle stability, Opt. Commun. 547 (2023) 129840.
[27] R.C. Thompson, Optical waves in layered media, J. Mod. Opt. 39 (1990) 147–148.
[28] Y. Chen, Broadband one-dimensional photonic crystal wave plate containing single-negative materials, Opt. Express. 18 (2010) 19920–19929.
[29] L. Qi, Z. Yang, F. Lan, X. Gao, Z. Shi, Properties of obliquely incident electromagnetic wave in one-dimensional magnetized plasma photonic crystals, Phys. Plasmas. 17 (2010).
[30] B. Tang, Z. Li, E. Palacios, Z. Liu, S. Butun, K. Aydin, Chiral-selective plasmonic metasurface absorbers operating at visible frequencies, IEEE Photonic Tech L. 29 (2017) 295–298.
[31] Y. Sharma, S. Prasad, V. Singh, Dispersion behavior of electromagnetic wave near the resonance in 1D magnetized ferrite photonic crystals, Opt. Quantum Electron. 50 (2018) 1–19.
[32] T.Q. Zhu, Y.M. Liu, J.T. Zhang, H.F. Zhang, The absorption properties of one-dimensional spherical photonic crystals based on magnetized ferrite materials, Annalen der Physik 535 (2023) 2200370.
[33] Y.R. Wu, Y.R. Dong, J. Xue, H.F. Zhang, A novel CPA-based layered photonic structure for multipurpose sensing applications, Opt. Laser Technol. 163 (2023) 109422.
[34] R.B. Goldfarb, Electromagnetic units, the Giorgi system, and the revised international system of units, Ieee Magn. Lett. 9 (2018) 1–5.
[35] R.B. Goldfarb, The permeability of vacuum and the revised International System of Units, Ieee Magn. Lett. 8 (2017) 1–3.
[36] A.H. Almawgani, D.N. Alhamss, S.A. Taya, I. Colak, A. Sharma, A.R. Alhawari, S. K. Patel, The properties of a tunable terahertz filter based on a photonic crystal with a magnetized plasma defect layer, Phys. Fluids 34 (2022).
[37] B. Lin, J.L. Wu, X.Y. Da, W. Li, J.J. Ma, A linear-to-circular polarization converter based on a second-order band-pass frequency selective surface, Appl. Phys. A-Mater. 123 (2017) 1–5.
[38] H. Jiang, H. Chen, H. Li, Y. Zhang, J. Zi, S. Zhu, Properties of one-dimensional photonic crystals containing single-negative materials, Phys. Rev. E—Statistical, Nonlinear, Soft Matter Phys. 69 (2004) 066607.
[39] I. Liberal, N. Engheta, Near-zero refractive index photonics, Nat. Photonics 11 (2017) 149–158.
[40] F.G. Xing, D. Zhang, H.F. Zhang, Polarization rotator between the linear polarization and the circular polarization based on the layered photonic structure, Annalen der Physik 534 (2022) 2200270.
[41] S. Kocaman, M.S. Aras, P.C. Hsieh, N.C. Panoiu, M.B. Yu, D.L. Kwong, C.W. Wong, Zero phase accumulation in negative-index photonic crystal superlattices, Nat. Photon. 5 (2011) 9344–9349.
[42] J.D. Adam, L.E. Davis, G.F. Dionne, E.F. Schloemann, S.N. Stitzer, Ferrite devices and materials, Ieee Trans. Microw Theory Tech. 50 (2002) 721–737.
[43] L. Xuan, X.H. Kong, J.M. Wu, Y.C. He, Z. Xu, A smoothly-connected crescent transverse gradient coil design for 50mT MRI system, Appl. Magn. Reson. 52 (2021) 649–660.
[44] Y. Ma, H. Zhang, Wide-angle energy steering and magnetic information detection-coding of stacked ferrite-based elements in the gradient magnetic domain, Opt. Laser Technol. 156 (2022) 108544.
[45] M.C. Onbasli, T. Goto, X. Sun, N. Huynh, C.A. Ross, Integration of bulk-quality thin film magneto-optical cerium-doped yttrium iron garnet on silicon nitride photonic substrates, Opt. Express. 22 (2014) 25183–25192.
[46] K. Xu, R.J. Spiegel, Y. Zhang, W.T. Joines, Q.H. Liu, Patch antenna with electrically tunable ferrite-ferroelectric bilayer, Prog Electromagn Res. (2014) 1773.
[47] M.N. Deeter, A.H. Rose, G.W. Day, Fast, sensitive magnetic-field sensors based on the Faraday effect in YIG, J. light. technol. 8 (1990) 1838–1842.
[48] Y. Chen, Z. Chen, J. Wei, Fe3O4 nanoparticle-based Janus photonic crystal microbeads with multiple fluorescence colors for information coding, ACS Appl. Nano Mater. 6 (2023) 14702–14709.
[49] D. Zhu, Y.H. Zhang, S.J. Liu, W. Chen, L. Zhu, S.J. Ge, Y.Q. Lu, Polychromatic dual-mode imaging with structured chiral photonic crystals, Nano Lett. 24 (2023) 140–147.